Materials Today Chemistry 46 (2025) 102719

Contents lists available at ScienceDirect

Materials Today Chemistry

journal homepage: www.journals.elsevier.com/materials-today-chemistry/

The antibacterial and anticorrosion activity of sodium alginate-chitosan cryogels and hydrogels loaded with *Satureja montana* essential oil and *Monarda didyma* hydrolate

Imane Haddadou [a], Amina Ami [b], Jonathan Gagnon [c], Claudiane M. Ouellet-Plamondon [a,*]

[a] *École de Technologie Supérieure, Université Du Québec, 1100 Notre-Dame West, Montréal, H3C 1K3, Canada*
[b] *Direction Centrale Recherche et Développement, SONATRACH, Avenue Du 1ernovembre, 35000, Boumerdes, Algeria*
[c] *Université du Québec à Rimouski, 300 Allée des Ursulines, Rimouski, Québec, G5L 3A1, Canada*

ARTICLE INFO

Keywords:
Chitosan
Sodium alginate
Cryogels
Essential oil
Hydrolate
Antibacterial activity
Anticorrosion

ABSTRACT

This study develops chitosan-alginate (CS/SA) cryogels incorporating *Satureja montana* essential oil (EO) and *Monarda didyma* hydrolate for antibacterial and anticorrosion applications. Cryogels with a CS:SA ratio of 3:1 achieved 78.7 % encapsulation efficiency (EE), driven by electrostatic interactions between chitosan's protonated amine ($-NH_3^+$) and alginate's carboxyl ($-COO^-$) groups, forming a dense polyelectrolyte network that entraps EO (FTIR/SEM evidence). Structural analysis revealed alginate-enhanced porosity (50–200 μm pores) and EO-induced densification, critical for controlled release. The cryogels inhibited *Staphylococcus aureus* (58.8 ± 2.3 %) and *Pseudomonas aeruginosa* (41.7 ± 3.0 %) and suppressed corrosion-associated strains: acid-producing bacteria (APB, 91.92 ± 0.16 %) and thiosulfate-reducing bacteria (BTR, 97.76 ± 0.27 %). Hydrolate-EO synergy enhanced anticorrosion performance, with CS/SA (3:1) cryogels retaining 90 % zinc on steel surfaces. This work demonstrates a sustainable strategy for dual-functional coatings, leveraging natural extracts to address industrial and environmental challenges.

1. Introduction

Hydrogels are three-dimensional, cross-linked polymer networks with excellent water-retaining capacity, making them highly suitable for a variety of biomedical and industrial applications [1]. These elastic materials can be synthesized from either natural polymers (such as alginate, cellulose, chitosan and collagen) or synthetic ones (polyamide, PVA, PVP, etc.) [2]. Compared to synthetic variants, natural polymer-based hydrogels offer several advantages, including biocompatibility, non-toxicity, biodegradability and reduced the ecological impact [3]. Thus, they are widely used in agriculture, food industry, biosensing and biomedical applications [4].

Among natural polymers, chitosan (CS) and sodium alginate (SA) are especially attractive due to their abundance, renewability, and favorable physicochemical properties [5]. Chitosan, a cationic polysaccharide derived from chitin, is well known for its biocompatibility, hydrophilicity and antibacterial properties [6]. It contains reactive amino groups that enable pH-responsive gelation through ionic crosslinking, typically requiring acidic conditions for solubility [7,8]. However, chitosan alone suffers from limitations, such as poor mechanical strength and rapid degradation under physiological conditions, which can restrict its use in long-term applications [9].

Sodium alginate (SA), a linear anionic polysaccharide derived from brown algae, exhibits excellent gel-forming ability in the presence of multivalent cations such as Ca^{2+}, Ba^{2+}, and Fe^{3+} [10,11]. Its gelation under mild conditions and relatively slower degradation rate make it a favorable counterpart to chitosan. Nevertheless, alginate lacks sufficient antimicrobial activity and mechanical robustness for many biomedical applications [12]. Thus, combining chitosan and alginate into a polyelectrolyte complex provides a synergistic platform, where electrostatic interactions between $-NH_3^+$ groups of chitosan and $-COO^-$ groups of alginate lead to the formation of mechanically stable, bioactive hydrogels with tunable degradation profiles. Together, they create robust, multifunctional hydrogels ideal for wound dressings, scaffolds for tissue regeneration and encapsulating bioactive agents [13–15].

Recent advances have shown that the stability and antimicrobial efficacy of hydrogels can be significantly enhanced through innovative

* Corresponding author.
E-mail address: claudiane.Ouellet-Plamondon@etsmtl.ca (C.M. Ouellet-Plamondon).

https://doi.org/10.1016/j.mtchem.2025.102719
Received 28 January 2025; Received in revised form 18 April 2025; Accepted 21 April 2025
Available online 29 April 2025

Abbreviations

CFU	colony forming unit
CS	chitosan
EDS	energy-dispersive X-ray spectroscopy
EE	encapsulation efficiency
EO	essential oil
EPS	extracellular polymeric substances
FTIR	Fourier transform infrared spectroscopy
Hyd	hydrolate
RT	room temperature
SA	sodium alginate
SD	standard deviation
SEM	scanning electron microscope

formulations and the incorporation of functional nanoparticles. For example, Brahmkhatri et al. demonstrated that while free curcumin undergoes rapid degradation, PVP-C and PVP-C nanoparticles significantly enhance stability, effectively prolonging curcumin's integrity in aqueous environments [16,17]. Li et al. developed a chitosan/alginate hydrogel embedded with silver nanoparticles (AgNPs) using tannic acid as a green reducing agent, achieving excellent antibacterial activity and controlled swelling behavior under varying pH conditions [18]. Similarly, Motelica et al. demonstrated that alginate films loaded with ZnO nanoparticles and citronella essential oil showed strong antibacterial performance and improved barrier properties, supporting their potential use in active food packaging [19]. Other studies have reported the use of thymol-loaded alginate-polylysine hydrogels with high antimicrobial activity across a wide pH range, as well as α-tocopherol-loaded chitosan/alginate hydrogels that promoted wound healing in vivo [20,21]. In addition, strategies such as incorporating poly(dimethylsiloxane) into chitosan-alginate polyelectrolyte complexes have yielded materials with enhanced mechanical strength and stability in physiological conditions [22]. Recent developments also include the creation of alginate-based zwitterionic double-network hydrogels with outstanding mechanical resilience, tear resistance, and dual sensitivity to pH and ammonia for real-time monitoring applications [23]. These findings emphasize the potential of chitosan and alginate-based hydrogels as multifunctional platforms when combined with nanoparticles or other modifiers, enhancing their stability, adaptability, and efficacy for antimicrobial and biomedical uses.

The ability of -chitosan–alginate-based hydrogels as encapsulation matrices for bioactive compounds, such as essential oils, and to protect these sensitive molecules from environmental degradation and to enable controlled release is particularly valuable for antimicrobial and anticorrosion applications. Essential oils (EO), derived from plant biomass including leaves, bark, seeds, and flowers, contain a complex mixture of volatile compounds such as monoterpenes, phenolics, and aldehydes [24,25]. These compounds exhibit significant anti-corrosive, antibacterial, antioxidant and anti-inflammatory properties, making them attractive candidates for integration into polymer-based delivery systems [26,27]. However, their lipophilicity and volatility make them highly susceptible to degradation when exposed to light, heat, or oxygen. Encapsulation in biopolymer matrices like hydrogels or cryogels provides a promising strategy to preserve their activity and enhance their therapeutic efficacy [28].

Alongside EO, hydrolates, aqueous co-products of steam distillation, have gained attention as sustainable, bioactive ingredients. Hydrolates contain trace amounts of EOs (less than 1 g/L) and a range of water-soluble components with antimicrobial potential [24,29,30]. Despite their ecological advantages and low toxicity, hydrolates remain underexplored in scientific research compared to essential oils. Their integration into hydrogel systems, particularly in synergy with EOs, offers an opportunity to enhance antimicrobial performance through combined hydrophilic and lipophilic activity [31].

Hydrogels and cryogels loaded with bioactive compounds have demonstrated strong antibacterial and anticorrosion performance, especially when used to prevent biofilm formation on industrial and biomedical surfaces [32,33]. Biocorrosion, driven by microbial activity, leads to serious structural degradation in pipelines, storage tanks, and medical implants, causing economic losses worldwide [34]. Several studies have highlighted the benefits of incorporating natural antimicrobials into hydrogel systems. For example, alginate hydrogels with 8 % thyme or clove EO exhibited potent antibacterial effects against *Escherichia coli* and *Bacillus cereus* [35]. Similarly, chitosan hydrogels co-loaded with tea tree oil and silver ions showed effective antimicrobial activity against *Pseudomonas aeruginosa*, *Staphylococcus aureus*, and *Candida albicans*, making them suitable for wound care [36]. Biopolymer coatings also hold great potential for corrosion inhibition and antifouling applications. For example, sodium alginate-based hydrogels with graphitic carbon nitride provided excellent protection for stainless steel surfaces, effectively preventing microbial and environmental degradation while demonstrating strong antibacterial properties against *Pseudomonas aeruginosa* [37]. Despite these promising results, further research is needed to optimize the performance of these materials in diverse environmental conditions to maximize their potential in practical applications.

The present work aims to develop and evaluate the antibacterial and anticorrosion effect of chitosan-alginate cryogels loaded with *Satureja Montana* EO and *Monarda didyma* hydrolate. *Satureja montana* (winter savory), a member of the mint family, is well-documented for its potent antiseptic, antibacterial, and antifungal activities, traditionally recognized by Native Americans [38]. Its EO has been successfully used both individually (diluted or not) and in combination with other components for antibacterial, antiviral, antifungal and anti-parasitic purposes, largely attributed to bioactive compounds such as carvacrol, alpha gamma terpenes, thymol, *p*-cymene, β-caryophyllene [24]. On the other hand, plants of the *Monarda* species, such as Red Bergamot, are rich in hydrophilic antimicrobial compounds, but remain underutilized in materials science research [39,40]. Previous studies have reported the antibacterial and corrosion-inhibiting potential of both winter savory EO [41] and *Monarda* hydrolate [40]; however, no studies to date have examined their combined use in cryogel matrices.

In this study, cryogels were developed with varying CS:SA ratios and loaded *Satureja montana* EO and *Monarda didyma* hydrolate to investigate their synergistic effects on microbial growth inhibition and corrosion resistance. The materials were characterized for their chemical, physical, morphological, and antibacterial properties. Antibacterial activity was assessed against clinically relevant aerobic pathogens (*Staphylococcus aureus* and *Pseudomonas aeruginosa*) isolated from waste water and environmental anaerobes associated with corrosion in industrial systems, including water pipes, cooling systems, storage tanks, and oil wells [42]. In this work, we intentionally selected environmental isolates to ensure relevance to real-world problems in wastewater treatment and oilfield corrosion mitigation. By integrating both hydrophilic and hydrophobic natural antimicrobials into a stable cryogel platform, this work proposes an innovative and sustainable strategy for mitigating microbial contamination and biocorrosion in diverse settings.

2. Experimental

2.1. Materials

Essential oil (EO) of winter savory (*Satureja montana*), and hydrolate (Hyd) of Red Bergamot or Scarlet Beebalm (*Monarda didyma*) were procured from Hunzaroma (Longueuil, QC, Canada). The composition of EO, as determined by chromatographic analysis, is detailed in Table S1. Sodium alginate (SA) was obtained from Acros organics (USA), while chitosan (CS, High molecular weight, viscosity of 1 wt% in 1 % acetic

acid at 25 °C is 800 cP, >75 % deacetylated), acetic acid and Polysorbate 80 (Tween-80) provided from Sigma-Aldrich (USA). All these chemicals were used without further purification. Water was purified using a Direct-Q 8UV Millipore system.

2.2. Hydrogels preparation

The different stock solutions of 2 wt % chitosan were prepared by dissolving 0.2 g of CS in 10 mL of 0.1 M acetic acid aqueous solution or hydrolate (with the pH adjusted using a few drops of diluted acetic acid) and stirring until a homogenous solution was obtained. In addition, 2 wt % alginate stock solutions were prepared by the same manner, by dissolving 0.2 g of sodium alginate in 10 mL of hydrolate or deionized water. The suspensions were stirred until the formation of homogenous solutions (Fig. S1–a). The chitosan/alginate (CS/SA) hydrogels were prepared by mixing different volume ratios of the stock solutions of SA and CS using ratios of (0:1), (1:3), (1:1), (3:1), and (1:0). The mixtures were then stirred at room temperature (RT) and the obtained hydrogels were immersed in a coagulation bath of 2 % wt. $CaCl_2$. The previous mixtures were frozen overnight at −20 °C, then lyophilized for 24 h using a Labconco freeze dryer and a highly porous solids were produced (Fig. S1–b). The hydrogels prepared with acetic acid and deionized water were coded as CS, CS/SA (3:1), CS/SA (1:1), CS/SA (1:3), and SA while those prepared with hydrolate were coded as Hyd-CS, Hyd-CS/SA (3:1), Hyd-CS/SA (1:1), Hyd-CS/SA (1:3), and Hyd-SA (Table S2).

2.3. Encapsulation procedure

A mixture of winter savory EO and Tween-80 (1:1, v:v) was sonicated (using an ultrasonic bath Branson 5200) for 30 min then magnetically stirred for 2 h. Subsequently, specified amounts of this mixture were gradually poured into the different CS/SA solutions while stirring to reach various ratios (0 % (control), 1 % and 2 %, v:v). The agitation was further continued overnight, at RT, to ensure the homogeneous dispersion of the EO (Fig. S2–a).

The encapsulation efficiency (EE) of winter savory EO in the cryogels was determined using a Cary 300 Bio (Varian) spectrophotometer. Briefly, 5 mg of cryogels was incorporated with 5 mL of aqueous hydrochloric acid solution (1 M) and boiled for 30 min. After cooling, 1 mL of ethanol was added to the mixture and centrifuged at 9000 rpm for 5 min [43]. The absorbance of the collected supernatant was measured at 280 nm against the blank (sample prepared from cryogel without EO and treated similarly as the EO-cryogel) (Fig. S2–b). The amount of EO entrapped in the cryogels was quantified from the regression equation: $y = 1.9042x + 0.908$, ($r^2 = 0.9977$), with y is absorbance intensity at 280 nm and x is EO concentration (g/mL). The percent EE was determined using the following formula [44]:

$$EE\ (\%) = (\text{initial EO amount} - \text{free EO amount}) \,/\, (\text{initial EO amount}) \times 100 \quad \text{(eq 1)}$$

2.4. Lyophilization

All the samples are processed into bulk cylinder by immersing various hydrogels in a 2 % wt. $CaCl_2$ coagulation bath for 10 min. They were then placed in cylindrical molds, frozen, and subsequently freeze-dried for 24 h to obtain a spongy structure.

2.5. Characterization

Their Fourier transform infrared spectroscopy (FTIR) spectra were recorded using a PerkinElmer Spectrum-2 spectrometer, equipped with a universal attenuated total reflectance (UATR) accessory. The measurements were performed in the spectral range of 400–4000 cm^{-1}, with a resolution of 4 cm^{-1} and an accumulation of 16 scans. The bulk density of the obtained cryogels (ρ) (in $g.cm^{-1}$) was calculated for each sample from the following formula:

$$\rho = W \Big/ \pi \times (D/2)^2 \times H \quad \text{(eq 2)}$$

where *W*, *D* and *H* are respectively the weight (g), the diameter (cm) and the thickness (cm) of samples.

The surface morphology of prepared cryogels was observed by Hitachi TM 3000 tabletop scanning electron microscope (SEM) at accelerating voltage of 15×kV and 50 × magnification to highlight macro-porous structures and changes in pore density following essential oil incorporation. Higher magnifications were deliberately avoided due to the charging effects and surface irregularities commonly associated with porous biopolymer matrices, which can significantly reduce image resolution and clarity [45,46].

2.6. Degradation behavior

The degradation study was performed for 120 days of incubation in wastewater, at neutral pH value. For this purpose, lyophilized and weighed chitosan/sodium alginates samples where immersed in the 100 mL of wastewater solutions. The samples were taken out, washed with distilled water, dried and weighted. The degradation percentages were calculated according to equation (3).

$$Degradation\ (\%) = \frac{W_i - W_f}{W_i} \times 100\% \quad \text{(eq 3)}$$

Where, W_i and W_f are the initial and the final weight (g), respectively. All experiments were repeated 3 times, and the values are reported as mean ± SD (n = 3).

2.7. Microbiological analysis

2.7.1. In vitro antibacterial activity

The antibacterial activity of the different hydrogel samples was tested against *Staphylococcus aureus* and *Pseudomonas aeruginosa*, representing Gram-positive and Gram-negative species, respectively, according to the ASTM E2149-01 standard [47]. These two strains were isolated from wastewater using a selective agar media then incubated for 24–72 h (details are mentioned in Fig. S3–a). The isolated strain was repeatedly subcultured to obtain a pure culture. The single colony of bacteria was suspended in a Luria Broth (LB) and then incubated at 37 °C for 16–18 h (Fig. S3–b). The bacterial culture was diluted to achieve a standardized concentration (10^8 CFU/mL) by adjusting its optical density at 600 nm to 0.08–0.12 with a Cary 300 Bio (Varian) spectrophotometer. Cryogels were sterilized by ultraviolet light irradiation for 20 min. 0.1 g cryogels were placed in sterile vials containing 9 mL of LB medium and 1 mL of bacterial suspension (10^6 CFU/mL) was added to each well. For bare EO, equivalent concentrations were prepared by emulsifying EO in sterile LB broth with the same volume of Tween 80. All experiments were conducted in triplicate including control broths with and without bacterial inoculation. The vials were then incubated at 37 °C with shaking at 250 rpm. After 24 h, the absorbance of the suspension at 600 nm (OD_{600}) was measured to evaluate the viability of the bacteria (eq (4)). In the other hand, 0.1 mL aliquots were withdrawn from each flask, diluted and plated on LB agar plates. The plates were incubated for 24–48 h at 37 °C and the bacterial colonies were counted.

$$\text{Bacterial growth reduction}\ (\%) = (A600_{control} - A600_{test}) \,/\, A600_{control} \quad \text{(eq 4)}$$

Where $A600_{control}$ and $A600_{test}$ are, the absorbance at 600 nm (OD_{600}) of the culture medium without and with cryogel after 24 h, respectively.

The antibacterial activity of selected cryogels against acid-producing bacteria (APB) and thiosulfate-reducing bacteria (BTR), isolated from

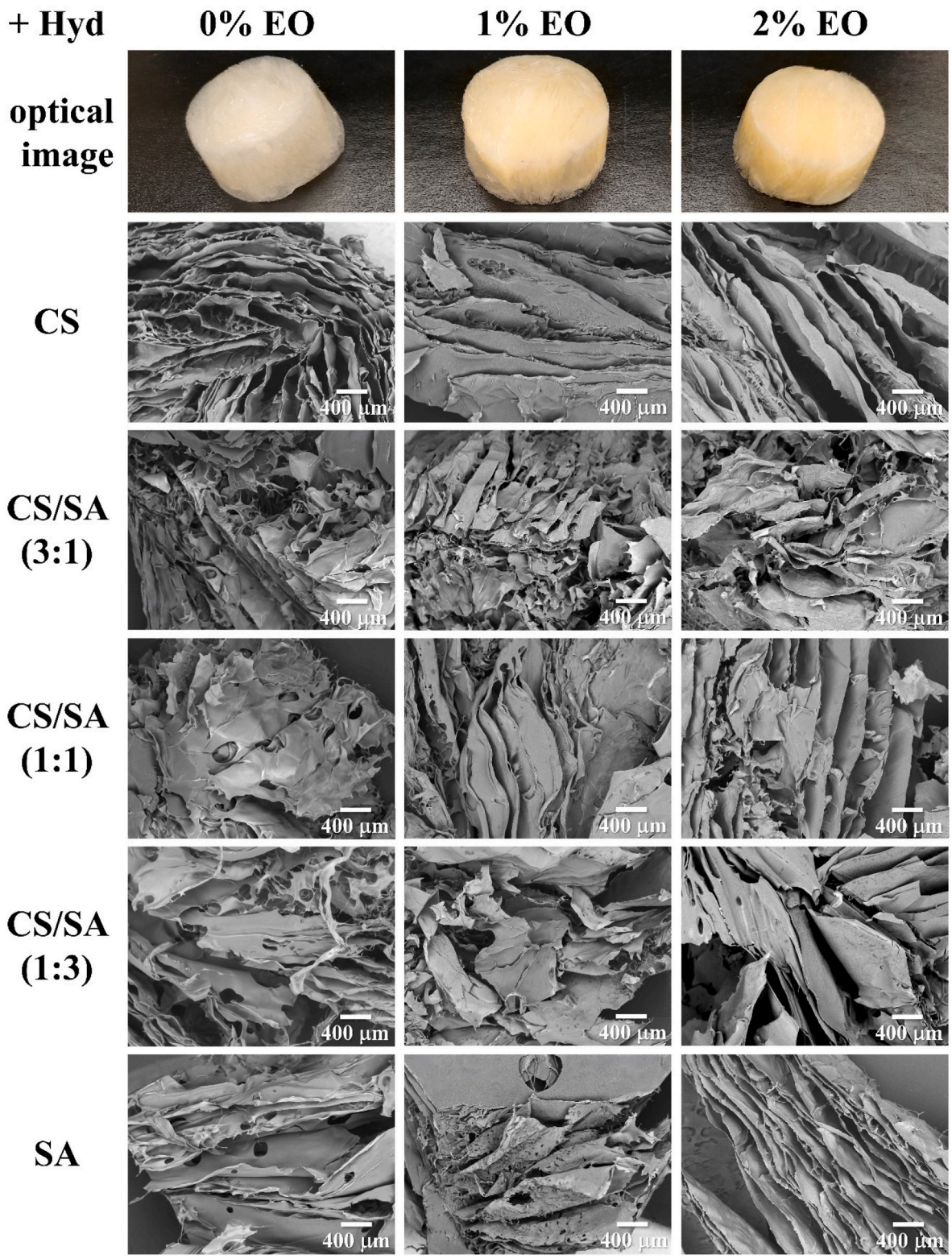

Fig. 1. Electron micrographs at magnification of 50 × and optical images of cryogels composed of chitosan (CS), sodium alginate (SA), and their mixtures (CS/SA in ratios of 3:1, 1:1, and 1:3) made with *Monarda didyma* hydrolate (Hyd) and different *Satureja montana* EO proportions (0, 1 and 2 %).

produced water collected from an oilfield in the southern Algerian Sahara, were assessed by the flask-shake method cited above. The isolation of APB and BTR consortia was carried out using specific liquid culture media for APB and BTR under anaerobic conditions at 40 °C over 28 days (Fig. S4). After enrichment in liquid media, the consortia were further isolated and purified on solid media by incubating anaerobically at 40 °C for 48 h. To prepare a fresh bacterial culture, single colonies were transferred into sterile Müller-Hinton broth and incubated at 40 °C for 48 h. The culture was then diluted to an optical density of 0.08–0.12 at 600 nm using a spectrophotometer (Cary 300 Bio, Varian) to standardize bacterial concentration (10^8 UFC/mL). Aliquots were serially diluted, mixed with pre-sterilized cryogels (UV-irradiated for 20 min),

and incubated at 40 °C under anaerobic conditions for 24 h. Bare EO was emulsified in sterile Müller-Hinton broth using an equal volume of Tween 80. Bacterial viability was evaluated by measuring the suspension's absorbance at 600 nm and counting colony-forming units (CFUs). For CFU determination, 0.1 mL of the suspension was plated on Müller-Hinton agar and incubated anaerobically at 40 °C for 48 h.

2.7.2. Anti-biocorrosion activity and weight loss assay

Zinc coatings are widely used to improve the corrosion resistance of steel in water. Therefore, zinc-plated steel flat washers were used as the metallic specimens in all tests conducted in this study. Prior to testing, washers were cleaned using deionized water, rinsed twice with ethanol, dried, and weighted to determine their initial weight. Immersion tests were conducted by placing each metallic specimen in a conical flask containing 100 ml of wastewater at RT for 120 days. The washers were either left uncoated or coated with various hydrogels (Hyd-CS, Hyd-CS/SA (3:1), Hyd-CS/SA (1:1), Hyd-CS/SA (1:3) and Hyd-SA), and then submerged in wastewater-filled flasks to evaluate the hydrogels' ability to inhibit biofilm formation and metal degradation. Before the immersion testing, the hydrogel-coated washers were placed in a coagulation bath of 2 % wt. $CaCl_2$ for 10 min. A sterile control was prepared by autoclaving the flask containing wastewater and uncoated washer at 121 °C for 15 min. This control was used to investigate the nature of corrosion in wastewater environment while excluding the influence of microbial deterioration (Fig. S5).

Surface morphology of all washer surfaces was observed with a SEM equipped with a Bruker XFlash 430-H energy-dispersive X-ray spectroscopy (EDS) detector for elemental analysis. After observation on SEM, the specimens were cleaned with ethanol to remove bacteria and biofilm products and weighed using an analytical balance to determine the post-immersion weight. The corrosion rate was calculated based on the weight loss of the specimens before and after immersion using equation (5).

$$\text{Corrosion rate} = \Delta W / (A \times \Delta T \times \rho) \quad \text{(eq 5)}$$

Where, ΔW is the weight loss (g) calculated as the difference between the initial weight (W_i) and the final weight (W_f) of the coupons ($\Delta W = W_i - W_f$), A is the exposed area (cm^2), ΔT is the exposure time (days) and ρ is the coupon density (g cm^{-3}).

2.8. Statistical analysis

All experiments were performed in triplicate, and the results were expressed as the mean ± standard deviation (SD). The data were analyzed using the ANOVA test with statistical significance assessed at $p = 0.05$.

For the weight loss tests, the effectiveness of the five hydrogel coatings in reducing corrosion was evaluated by comparing the corrosion rates of each coated sample (five coating types × two EO ratios) with those of the uncoated control in non-sterile wastewater. These comparisons were performed using a two-sample Student's t-test with Welch's correction. To account for multiple comparisons (10 total t-tests), the significance level was adjusted to $p = 0.005$ using the Bonferroni correction. The null hypothesis stated that the hydrogel coatings did not reduce corrosion rates, whereas the alternative hypothesis proposed that the coatings significantly reduced corrosion rates compared to the uncoated control. Additionally, the impact of EO concentration was evaluated by comparing the corrosion rates of each hydrogel-coating between the two EO ratios. These comparisons were also conducted using two-sample Student's t-test with Welch's correction, and significance was determined at $p < 0.05$.

Table 1
Encapsulation efficiency (EE) of *Satureja montana* EO into cryogels with and without *Monarda didyma* hydrolate. Values represent mean ± SD.

Cryogel composition	With hydrolate		Without hydrolate	
	1 % EO	2 % EO	1 % EO	2 % EO
CS	50.7 ± 2.2	65.4 ± 5.1	47.3 ± 1.2	61.6 ± 1.3
CS/SA (3:1)	62.2 ± 2.3	78.7 ± 3.2	57.2 ± 3.4	73.3 ± 1.1
CS/SA (1:1)	43.1 ± 1.2	59.6 ± 3.0	42.2 ± 3.2	56.9 ± 2.1
CS/SA (1:3)	35.5 ± 1.6	51.5 ± 4.8	33.1 ± 1.3	51.5 ± 2.4
SA	21.5 ± 1.8	40.4 ± 2.6	19.1 ± 2.9	37.2 ± 2.2

3. Results and discussion

3.1. Morphological characterization of cryogels

The SEM images in Fig. 1 reveal notable differences in the microstructure of cryogels formulated with varying ratios of CS and SA, alongside varying concentrations of essential oil (EO) and the inclusion of the hydrolate. The cryogels exhibit a sheet-like layer structure with porosity level varying based on the precursor's nature and their ratio. While pure CS cryogels showed limited porosity, increasing SA content in CS/SA composite cryogels leads to a more open and porous structure, due to SA's hydrophilic and network-forming capabilities [12,48]. This aligns with findings in hydrogels and biopolymeric scaffolds, where the addition of SA promotes a more open and interconnected porous architecture [44,49,50].

Incorporation *Satureja montana* EO (at 1 % and 2 % v/v) into the cryogels resulted in a visibly more compact sheet structure with fewer, less-defined pores. The presence of this hydrophobic agent leads to aggregation and stacking of the polymer sheets, likely due to limited compatibility between the hydrophobic EO and the hydrophilic cryogel matrix [51]. This structural densification can be attributed to the interference of EO with the polymer network's expansion during the freeze-thaw cycle, which restricts pore formation [52]. Higher EO concentrations (2 %) further amplify this effect, creating the densest observed morphology and indicating a proportional relationship between EO concentration and structural compactness. Moreover, an observable color change from white to a darker yellow was noted as the EO concentration increased, consistent with the findings of Dinu et al. (2021), where EO-loaded cryogels exhibited color changes proportional to EO content due to the EO's intrinsic color [53].

Interestingly, the presence or absence of *Monarda didyma* hydrolate does not visibly affect the morphology or color of the cryogels, suggesting that the addition of hydrolate does not alter the internal structure at this magnification, compared to the marked effects induced by EO and compositional variations of CS and SA (Fig. S6). This stability could be attributed to the compatibility of hydrolate's aqueous nature with the polymeric matrix.

3.2. Encapsulation of EO

The retention of EO into polymeric structures depends on several factors and determining the encapsulation efficiency is crucial as it affects the properties of the final material (stability, EO release and bioactivity). This study investigated the effect of the cryogel compositions, EO ratios, and the presence of *Monarda didyma* hydrolate on the encapsulation efficiency of *Satureja montana* EO into cryogels composed of CS, SA, and their mixtures (CS/SA in ratios of 3:1, 1:1, and 1:3) (Table 1).

Increasing the essential oil concentration significantly improved the encapsulation efficiency ($p < 0.0001$), suggesting that higher EO quantity enhance interactions with the polymer matrix, leading to better encapsulation. However, the extent of this improvement depended on the specific cryogel composition and the presence of the hydrolate. While the use of the hydrolate seemed to slightly enhance the

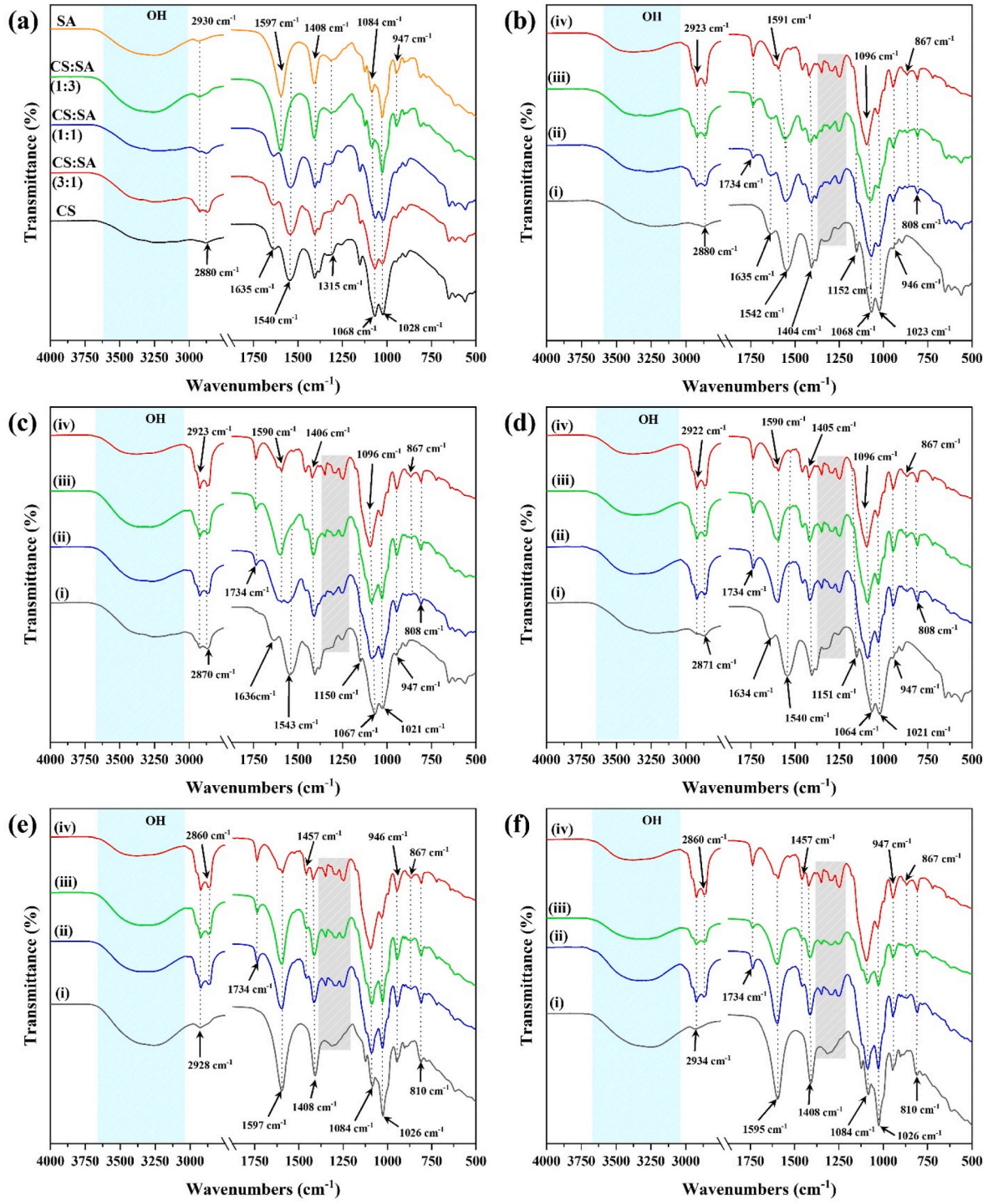

Fig. 2. FTIR of cryogels made with varying proportions of chitosan (CS) and sodium alginate (SA), without (a) and with *Satureja montana* essential oil (EO): CS (b), CS:SA (3:1) (c), CS:SA (1:1) (d), CS:SA (1:3) (e) and SA (f). The cryogel without EO (i), cryogel with 1 % (ii) and 2 % EO (iii), and pure *Satureja montana* essential oil (iv). All the cryogels are made without *Monarda didyma* hydrolate.

encapsulation efficiency, the change was statistically insignificant ($p > 0.05$). The hydrolate likely acted as a stabilizing agent, enhancing compatibility between the hydrophilic polymer matrix and the hydrophobic EO. This synergy may be attributed to water-soluble bioactive compounds in the hydrolate, which could interact with both the polymer network and the EO, thereby facilitating retention within the cryogel. Furthermore, the functional groups present in the hydrolate may form hydrogen bonds and electrostatic interactions with the cryogel polymers, further supporting the encapsulation process. These findings align with previous studies, which demonstrate that higher EO concentrations improve encapsulation efficiency due to increased interaction with the encapsulating material [54].

In the other hand, the encapsulation efficiency was strongly dependent on the composition of the cryogels and the nature of the polymers forming them ($p < 0.0001$). Encapsulation efficiency ranged from 47.3 % to 65.4 % when EO was encapsulated into chitosan, while lower efficiency was observed with alginate (19.1 %–40.4 %). The highest encapsulation efficiency was recorded with the combination CS/SA

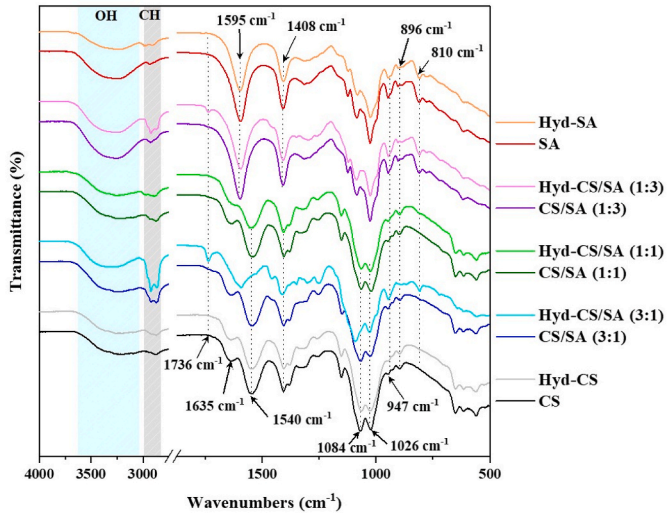

Fig. 3. FTIR of cryogels composed of chitosan (CS), sodium alginate (SA), and their mixtures CS/SA in ratios of 3:1, 1:1 and 1:3, in presence and absence of hydrolate (Hyd).

(3:1) with the hydrolate and 2 % EO, reaching up to 78.7 %. This high encapsulation efficiency is due to the strong electrostatic interaction between the carboxylate anions of SA and the ammonium cations of CS, forming a polyelectrolyte complex. This interaction leads to significant entrapment of the EO and reduces leakage, as the mechanical strength and structural integrity provided by chitosan help reduce the porosity of alginate [55,56].

3.3. Chemical composition analysis

ATR-FTIR spectra (Fig. 2, Table S3) provide detailed insight into the molecular interactions involved in cryogels formation. Spectral profiles of pure CS display characteristic broad O–H/N–H stretching around 3240 cm^{-1}, corresponding to intra- and intermolecular hydrogen bonding. The amide II band at 1540 cm^{-1} reflects N–H bending while the amide III band at 1318 cm^{-1} corresponds to C–N stretching. Additionally, the region between 1023 and 1152 cm^{-1} is associated to C–O–C stretching vibrations from the glucosamine backbone [57]. In contrast, pure SA exhibits distinct asymmetric and symmetric carboxylate stretching vibrations at 1597 and 1408 cm^{-1}, respectively, as well as a broad O–H band at 3230 cm^{-1} [58]. These reference spectra confirm the expected functional group distributions in the individual biopolymers (Fig. 2a).

In CS/SA cryogels, blending results in notable spectral shifts and band modulations, indicating interactions between the two polymers. As SA content increases, the intensity of aliphatic C–H bands at 2919 and 2880 cm^{-1} becomes more pronounced, alongside a broader hydroxyl stretching band centered around 3200 cm^{-1}. In SA-rich formulations, carboxylate peaks dominate the spectra, particularly in CS/SA (1:3) blends, reflecting the compositional influence of SA [59,60]. Additionally, the amide I band of CS (typically at 1635 cm^{-1}) overlaps with SA's carboxylate vibration, forming a broadened band in the 1600 cm^{-1} range, particularly pronounced in the CS/SA (3:1) formulation. This observation strongly supports the formation of polyelectrolyte complexes through electrostatic interactions between the protonated amine groups of CS and the carboxylate groups of SA, with concomitant displacement of sodium ions (Na^{+}) from the alginate structure. The reduced sodium content further corroborates this mechanism [61,62].

EO incorporation preserved the polymer backbone but introduced subtle shifts (e.g., O–H at 3264 cm^{-1}, C–H at 2928 cm^{-1}) and a carbonyl peak (1734 cm^{-1}), aligning with EO's γ-terpinene and carvacrol components (Table S4) [52,63]. These changes reflect non-covalent interactions (hydrogen bonds, van der Waals forces) [64], enhancing network density without disrupting structural integrity. Minimal spectral alterations in CS-dominated systems highlight the importance of SA's carboxylate groups in mediating additive integration (Fig. 2b–f).

Hydrolate integration induced formulation-dependent interactions. CS/SA (3:1) cryogels showed reduced O–H intensity, and intensified C–H vibrations, indicative of synergistic hydrogen bonding and hydrophobic interactions between hydrolate phenolics and alginate's functional groups (Fig. 3). A new carbonyl peak (1739 cm^{-1}) and reduced conjugated carboxylate/amide I (1635 cm^{-1}) suggest esterification or physical entrapment, consistent with prior studies on phenolic-polysaccharide interactions [65]. Intermediate ratio, CS/SA (3:1), exhibited weaker effects, underscoring SA's critical role in hydrolate binding via ionic and hydrogen-bonding sites. Collectively, the data elucidate how polymer ratios and additive chemistry govern cryogel interactions, with CS/SA (3:1) optimized for hydrolate and EO binding, balancing stability and functionality.

3.4. The density of cryogels

The effect of the essential oils and the hydrolate on the density of cryogels composed of chitosan, alginate, and their mixtures was investigated (Table 2). Cryogels made solely from chitosan exhibit a denser structure (≅ 0.033 g cm^{-1}), while the addition of alginate decreases the density, an effect that is statistically insignificant ($p = 0.97531$). The use of the hydrolate results in a slight, statistically insignificant difference in density ($p = 0.33533$), leading to a less dense structure. Conversely, the addition of essential oils significantly increases the density across all polymer mixtures ($p < 0.0001$). The effect of adding EO is more pronounced compared to the use of the hydrolate in the cryogel formulation. These findings align with existing literature on cryogels and their applications [66,67]. Cryogels are known for their highly porous structures and the addition of essential oils, which are hydrophobic, likely increases the density by reducing the overall porosity of the cryogel matrix [68]. Conversely, the incorporation of the hydrolate, which are colloidal suspensions of essential oil droplets in water, may introduce additional water content, thereby reducing the density [69].

3.5. Biological activity of cryogels

3.5.1. In vitro antibacterial activity

Fig. 4a and b and Figure S7 illustrate the bacterial growth reduction

Table 2
Bulk density of cryogels prepared with different proportions of chitosan (CS) and sodium alginate (SA), with and without *Monarda didyma* hydrolate, at varying concentrations of *Satureja montana* essential oil (0 %, 1 %, and 2 %).

Hyd	EO (%)	CS	CS:SA (3:1)	CS:SA (1:1)	CS:SA (1:3)	SA
+	0	0.0330 ± 0.0015	0.0303 ± 0.0002	0.0327 ± 0.0024	0.0309 ± 0.0008	0.0301 ± 0.0005
	1	0.0512 ± 0.0009	0.0499 ± 0.0006	0.0478 ± 0.0007	0.0449 ± 0.0018	0.0434 ± 0.0018
	2	0.0654 ± 0.0019	0.0642 ± 0.0013	0.0629 ± 0.0010	0.0616 ± 0.0006	0.0607 ± 0.0004
–	0	0.0412 ± 0.0002	0.0404 ± 0.0002	0.0396 ± 0.0004	0.0387 ± 0.0006	0.0370 ± 0.0011
	1	0.0516 ± 0.0005	0.0508 ± 0.0009	0.0496 ± 0.0018	0.0484 ± 0.0019	0.0466 ± 0.0025
	2	0.0707 ± 0.0036	0.0687 ± 0.0037	0.0678 ± 0.0040	0.0665 ± 0.0042	0.0655 ± 0.0045

Bulk density value (mean ± SD; n = 3) in g.cm^{-1}.

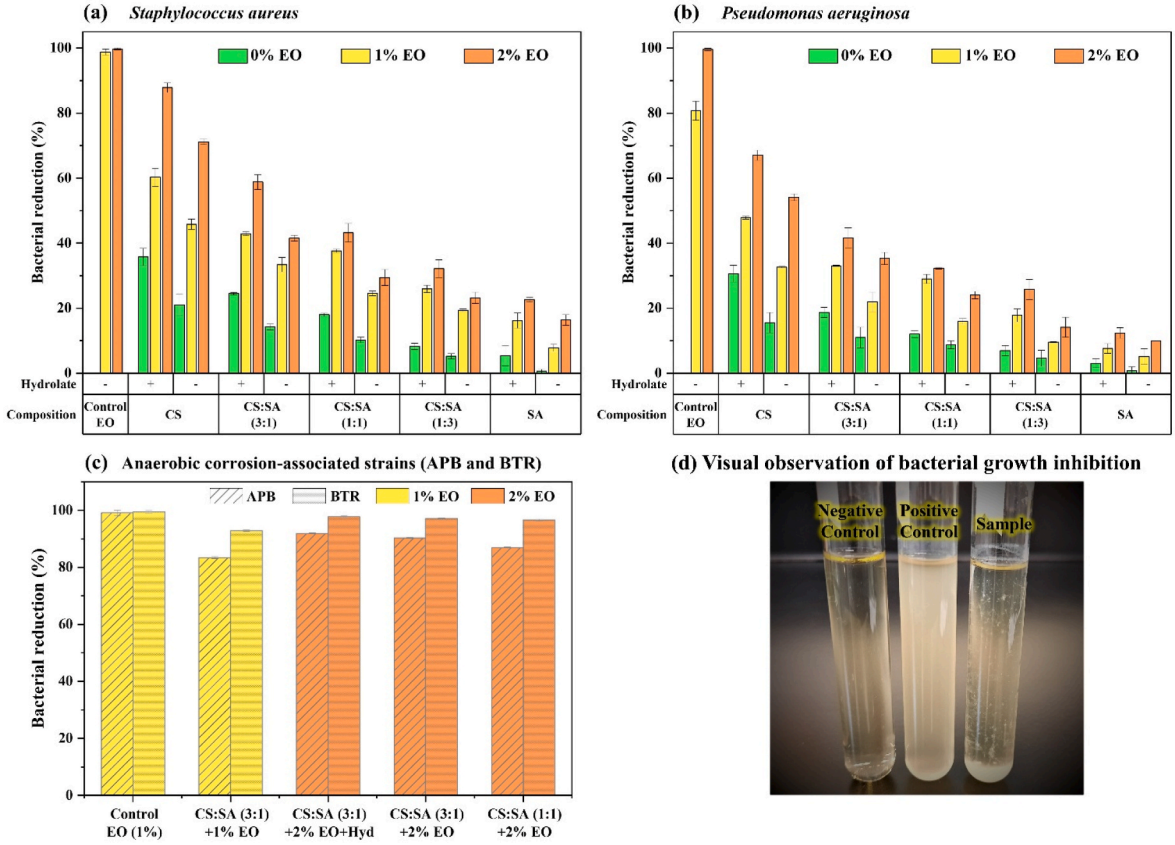

Fig. 4. The bacterial growth reduction by different cryogels (mean ± SD; n = 3), with (+) and without (−) hydrolate and various EO proportions against *S. aureus* (a), *P. aeruginosa* (b) and APB and BTR (c).

of various cryogels against *Staphylococcus aureus* and *Pseudomonas aeruginosa*. Cryogels were tested both with and without the hydrolate and at different EO concentrations (0 %, 1 %, and 2 %). The results indicate that cryogels based on chitosan (CS), either alone or in combination with sodium alginate (SA) at a 3:1 ratio, exhibited the strongest antibacterial effects against both *S. aureus* and *P. aeruginosa*. In contrast, SA-based cryogels alone were notably less effective. The incorporation of hydrolate improved antibacterial performance, reducing bacterial viability further, likely due to its additional bioactive compounds [31].

The addition of EO significantly enhanced the antibacterial activity against *S. aureus* and *P. aeruginosa* ($P < 0.0001$). A clear dose-dependent effect was observed, with higher EO concentrations leading to greater bacterial reduction. *Satureja montana* EO is rich in antimicrobial compounds such as terpenes and phenolics, which are known to disrupt microbial membranes and interfere with cellular functions [70,71]. *Staphylococcus aureus* was more sensitive to the EO-loaded cryogels than *Pseudomonas aeruginosa,* consistent with earlier studies [72,73]. To evaluate the impact of encapsulation, cryogels were compared with bare EO at equivalent concentrations (1 % and 2 % v/v). Although bare EO showed higher immediate antimicrobial activity, cryogels provided a more sustained effect over 24 h, likely due to the controlled release of EO from the cryogel matrix. Among all tested formulations, the CS:SA (3:1) cryogel containing hydrolate and 2 % EO exhibited the highest antibacterial efficacy, with 87.8 ± 1.4 % inhibition of *S. aureus* and 41.7 ± 3.1 % inhibition of *P. aeruginosa*. These findings align with previous studies that demonstrate the synergistic effects of chitosan and EO in enhancing antibacterial performance [74].

3.5.2. *In vitro antibacterial activity against biocorrosion-causing strains*

To evaluate the combined effects of the hydrolate addition, EO concentration, and the polymers ratio on antibacterial efficacy against biocorrosion-related strains (APB and BTR), five cryogel formulations were tested under anaerobic conditions. These included three cryogels with varying CS/SA ratios (1:3, 1:1, and 3:1), each containing hydrolate and 2 % EO, one formulation with a 1 % EO, and another with a CS/SA ratio of 3:1 and 2 % EO but without hydrolate. This experimental design allowed evaluation of the individual and combined impact of each parameter on antimicrobial performance.

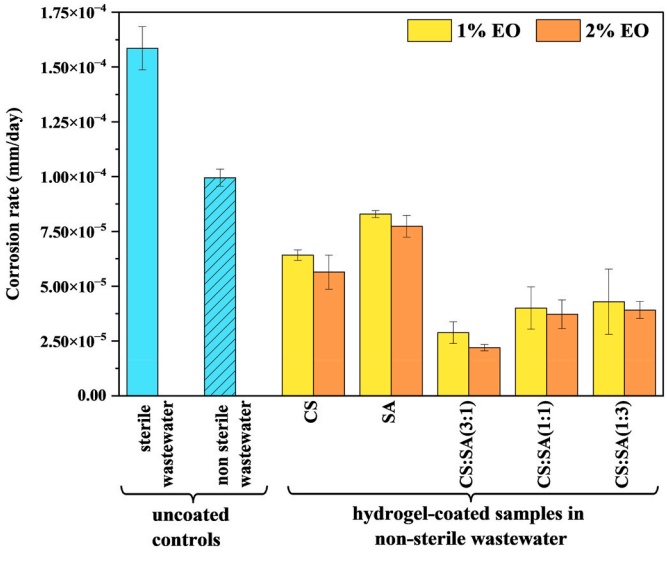

Fig. 5. Corrosion rates of uncoated and hydrogel-coated coupons, in sterile and non-sterile wastewater.

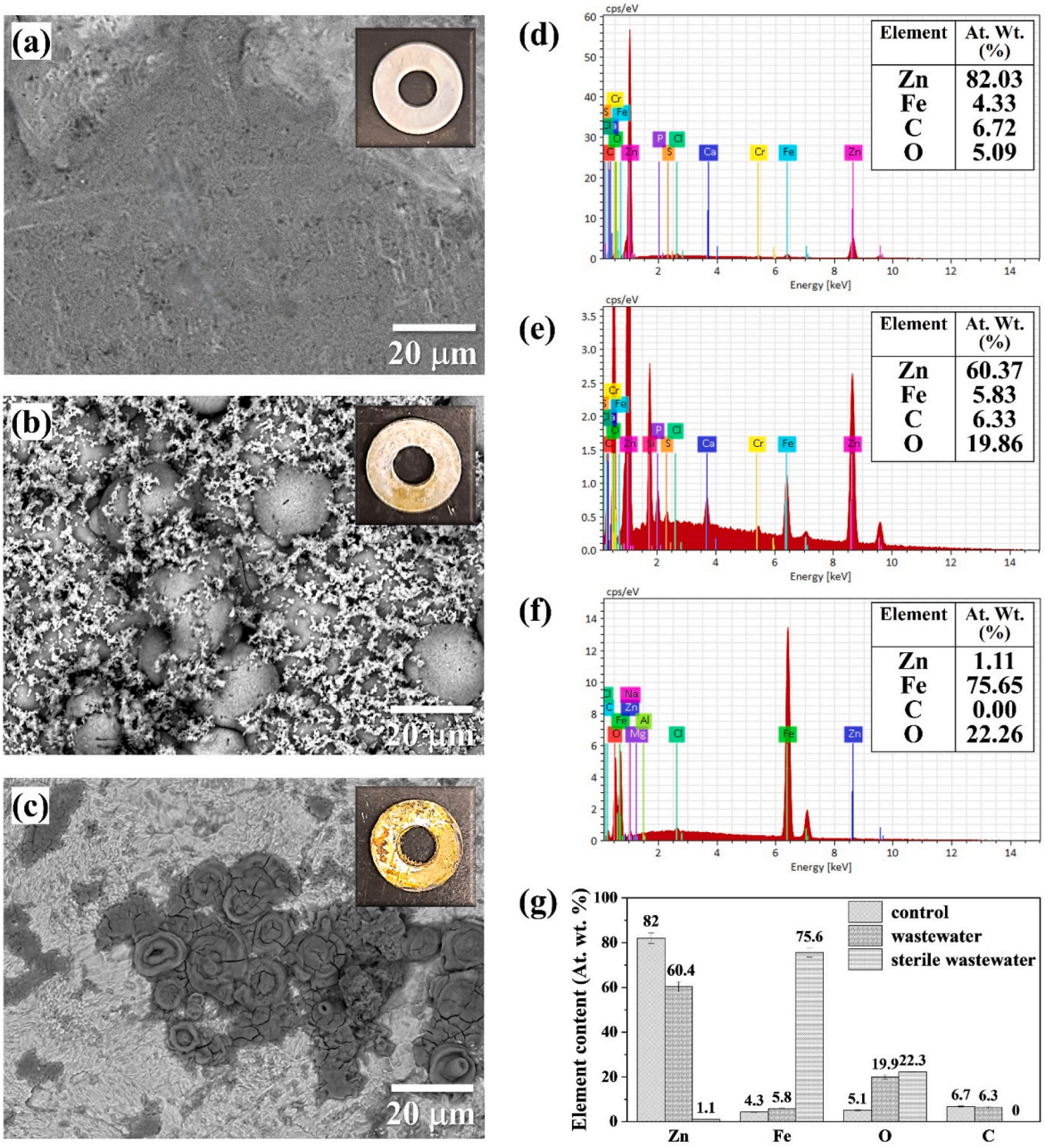

Fig. 6. SEM and optical image (inset) of zinc-plated steel coupons surface before (a) and after immersion for 120 days in nonsterile (b) and sterile (c) wastewater, and their corresponding EDS data respectively (d, e, and f). Comparison of the elemental composition data before and after immersion in sterile and non-sterile wastewater.

While bare EO at 1 % showed high immediate antibacterial activity (**99.1 ± 1.0 %** for APB and **99.5 ± 0.5 %** for BTR), the cryogels provided a more sustained effect over 24 h. Among all formulations, the CS: SA (3:1) cryogel 2 % EO and hydrolate, demonstrated the highest antibacterial efficacy, inhibiting APB and BTR growth by 91.92 % ± 0.16 and 97.76 % ± 0.27, respectively, with a notably stronger effect against BTR (Fig. 4c). These results confirm that the inclusion of both EO and hydrolate enhances the antimicrobial activity of the cryogels, supporting their potential application in preventing microbiologically influenced corrosion.

3.6. Anti-biocorrosion activity and weight loss assay

3.6.1. Corrosion inhibition efficacy

Fig. 5 shows the corrosion efficacy measured by the corrosion rate of hydrogel coatings in reducing corrosion rates of metal samples in non-sterile wastewater compared to uncoated controls. The uncoated control under sterile conditions exhibited the highest corrosion rate (~1.6 $\times 10^{-4}$ mm/day), significantly higher than the rate observed under non-sterile conditions ($p = 0.0041$; Fig. S8). Hydrogel-coated samples showed significantly lower corrosion rates in non-sterile wastewater compared to uncoated controls ($p < 0.0025$; Fig. S9). Among the tested hydrogel formulations, the CS/SA mixture at a 3:1 ratio provided the highest corrosion protection, likely due to the complementary properties of the two polymers: alginate provides structural stability, while

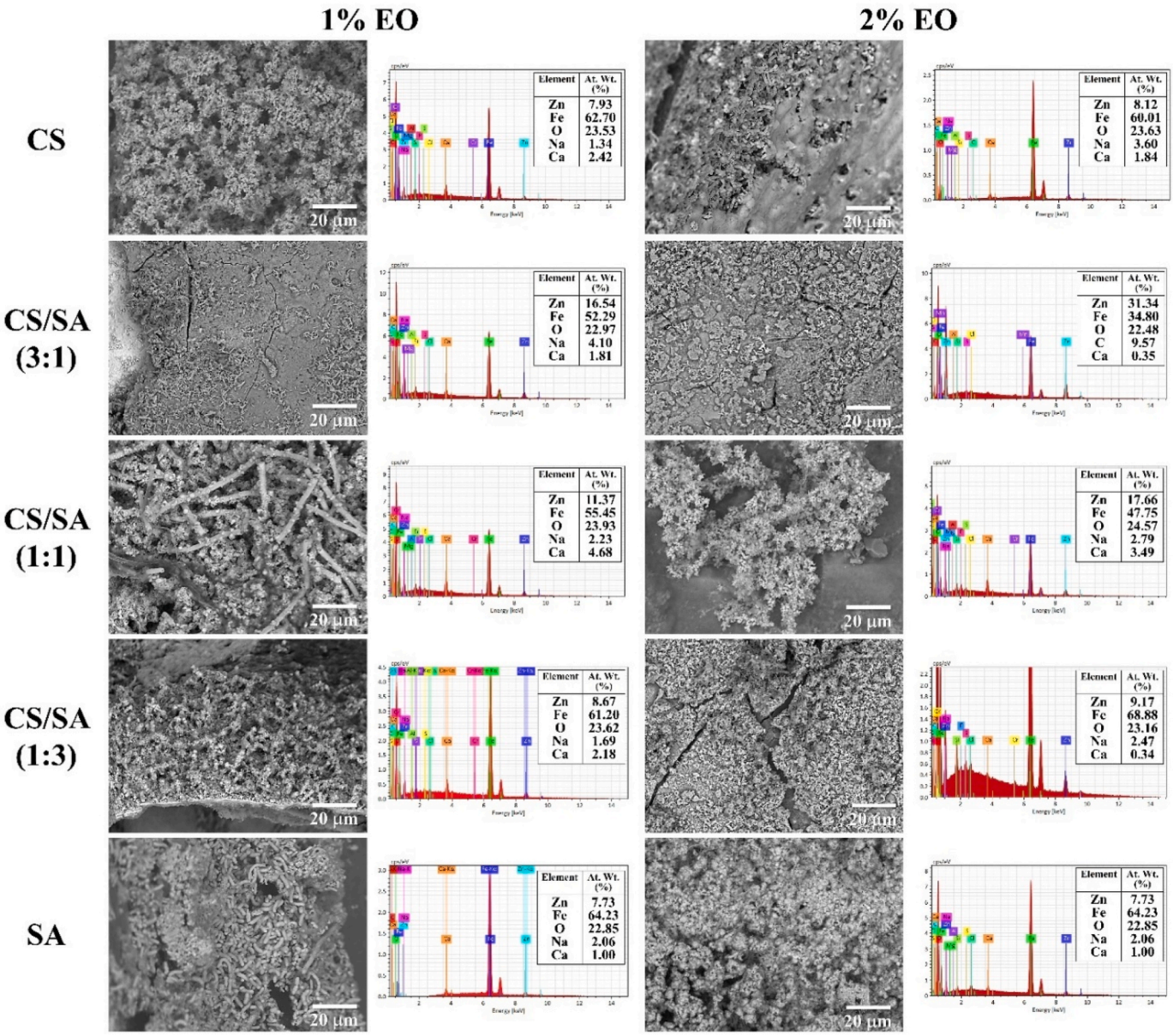

Fig. 7. SEM micrographs and the corresponding EDS spectra of elemental composition of the biofilm/corrosion products on the hydrogel-coated surface after 120 days of immersion in non-sterile wastewater.

chitosan contributes antimicrobial activity. These results align with previous studies demonstrating that natural polymer-based coatings act as effective corrosion barriers due to their film-forming ability and chemical stability [75]. Similarly, Gallegos-Melgar et al. also reported superior corrosion protection by chitosan-alginate films compared to chitosan alone, highlighting the benefits of polymer intermixing [76].

Incorporation of 2 % EO further improved corrosion resistance, with trends indicating enhanced barriers and antimicrobial properties, although individual sample differences were not always statistically significant ($p > 0.05$; Fig. S8). These findings are consistent with prior reports suggesting that EO incorporation reduces biofilm formation and enhances coating hydrophobicity, thereby mitigating microbiologically influenced corrosion [77].

3.6.2. *Characterization of the uncoated coupons surface*

Fig. 6 illustrates the surface morphology of the zinc-plated steel coupons under different immersion conditions after 120 days compared to the control (coupon before immersion). Initially, the surface of the zinc-plated steel coupon was smooth and flat, with no attached bacteria or visible signs of corrosion (such as pitting or cracking) (Fig. 6a). Corresponding EDS analysis (Fig. 6d) confirmed the high zinc content (82.0 ± 2.4 %), with a minor amount of iron, carbon, and oxygen, indicating an unaltered protective zinc coating and minimal initial oxidation or contamination.

After 120 days in wastewater, the surface showed significant degradation, with a rough texture and a biofilm of microorganisms and corrosion products (Fig. 6b). EDS analysis (Fig. 6e) revealed a notable reduction in zinc content (60.4 ± 2.2 %) and an increase in oxygen (19.86 ± 0.89 %), indicating active zinc oxidation and biofilm-associated corrosion. Under sterile conditions, the corrosion pattern was different. The surface remained rough with localized cracked oxide crusts but lacked the biofilm observed in non-sterile environment (Fig. 6c). EDS data (Fig. 6f) indicated a drastic reduction in zinc (1.11 ± 0.12 %) and a significant increase in iron (75.7 ± 2.1 %), showing that most of the zinc layer had corroded via galvanic process, exposing the underlying steel to the corrosive environment [78].

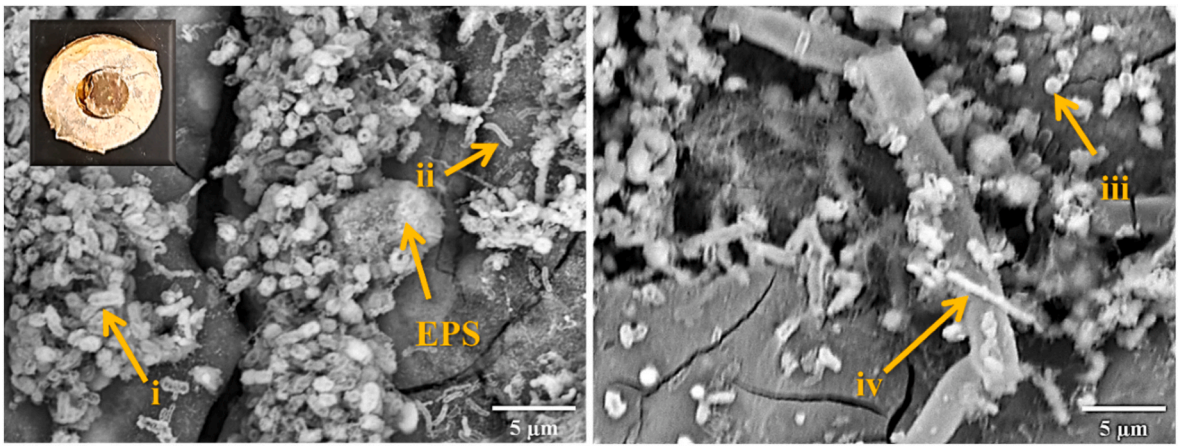

Fig. 8. SEM micrographs of biofilms on the surface of hydrogel-coated coupons at ×5k magnification. Spirals (i), bacilli (ii), cocci (iii) and filaments (iv), extracellular polymeric substance (EPS). Inset: optical image.

In fact, in abiotic environments, corrosion occurs primarily through electrochemical reactions with dissolved ions. However, microorganisms may not always enhance corrosion. Notably, certain species may exert protective effects that slow down the process [79]. This may explain the higher corrosion rates observed in abiotic conditions for uncoated controls, where the absence of microbial activity allows electrochemical reactions to dominate.

3.6.3. *Characterization of the hydrogel-coated coupons surface*

After 120 days of immersion in wastewater, SEM analysis revealed the formation of a biofilm layer on all hydrogel-coated zinc-plated steel coupons, as summarized in Fig. 7. At higher magnification (Fig. 8), diverse microbial morphologies, including spirals (i), bacilli (ii), cocci (iii) and filaments (iv), were observed embedded within an extracellular polymeric substance (EPS), consistent with a mature biofilm. EDS analysis of the biofilm indicated elevated levels of Fe and O alongside reduced Zn, suggesting the occurrence of biocorrosion. Biofilms create localized microenvironments with altered pH, oxygen gradients, and metabolic by-products, which accelerate metal degradation by disrupting the protective zinc layer and exposing the underlying steel to corrosive agents [80].

After removing the hydrogel coatings, SEM analysis of the exposed metallic surfaces displayed significant differences in surface degradation across samples, including cracking and pitting, which correlate with hydrogel composition (Fig. 9). These observations align with literature linking biofilm-associated biocorrosion to microbial activity and EPS formation, which facilitate ion transport and metal dissolution [81].

Among the tested formulations, CS hydrogel-coated surfaces displayed pronounced cracking and localized corrosion, reflected in the EDS data by significant iron enrichment and reduced zinc levels. This reflects poor corrosion protection, dominated by Fe oxidation, and aligns with higher weight loss measurements, indicating the limited protective efficacy of CS alone. Similarly, SA hydrogel-coated samples exhibited more extensive cracking, granular deposits, and localized corrosion. EDS data revealed reduced zinc content and elevated iron content, with weight loss measurements being the highest among all coatings, confirming the limited efficiency of SA in reducing material degradation. The high water permeability and susceptibility of SA to polymer degradation in harsh wastewater likely undermine its protective performance [82].

In contrast, CS/SA mixtures, particularly at 3:1 ratio, showed smoother surfaces with minimal cracks and pitting. These coatings retained higher Zn content and exhibited lower Fe content, indicating better resistance to corrosion. Weight loss measurements confirmed their superior performance, likely due to chitosan's barrier properties and the stabilizing effect of sodium alginate [83].

Incorporating 2 % EO into the hydrogel matrix further enhanced corrosion resistance. SEM images showed smoother surfaces with minimal cracking compared to 1 % EO formulations. EDS data revealed higher Zn and lower Fe levels, while weight loss measurements demonstrated significantly reduced degradation. The antimicrobial and hydrophobic properties of EO likely suppressed biofilm formation and microbial-induced corrosion, limiting ion transport to the metal surface [84].

The combined SEM, EDS, and weight loss analyses confirm that the CS/SA (3:1) hydrogel formulation provides the best corrosion protection, with minimal surface damage, low weight loss, high Zn retention, and reduced Fe oxidation. Incorporating 2 % essential oil further enhances these protective properties, highlighting the synergy between chitosan's film-forming capacity and the antimicrobial action of EO. Conversely, coatings dominated by sodium alginate (CS/SA 1:3 and SA) exhibit the poorest performance, as reflected in higher surface degradation, lower Zn levels, higher Fe content, and significant weight loss. These results emphasize the importance of optimizing hydrogel composition and incorporating functional additives to mitigate corrosion effectively.

3.7. *Degradation behavior of cryogels*

The degradation stability of the cryogels was evaluated by monitoring mass loss after four months of immersion in wastewater (Fig. 10). The results revealed a strong correlation between polymer composition and degradation behavior. CS-based formulations, including Hyd-CS and Pure CS, showed the highest mass loss (85.4 ± 1.1 % and 79.6 ± 1.2 %, respectively), indicating limited long-term stability. In contrast, SA-rich cryogels demonstrated significantly lower degradation. Since ionically crosslinked alginate hydrogels do not specifically degrade but undergo slow, uncontrolled dissolution, the coagulation process in $CaCl_2$ likely enhanced structural integrity by forming stable "egg-box" complexes between SA and Ca^{2+}, as observed in prior studies [85,86]. The Hyd-CS/SA (1:3) formulation containing 2 % EO exhibited the greatest stability, with a mass loss of only 35.1 ± 1.3 %.

A consistent trend was observed: increasing the SA content reduced the degradation rate. As reported in literature, alginate degrades more slowly than chitosan [87]. Formulations with CS/SA ratios of 1:1 or lower retained more than 50 % of their original mass, consistently outperforming CS-dominant systems. A modest improvement in degradation resistance was also noted with higher essential oil (EO) concentrations, suggesting a stabilizing effect. Hydrolate incorporation contributed to slightly enhanced structural integrity but to a lesser extent than SA or EO.

These findings suggest that both SA and EO contribute to cryogel

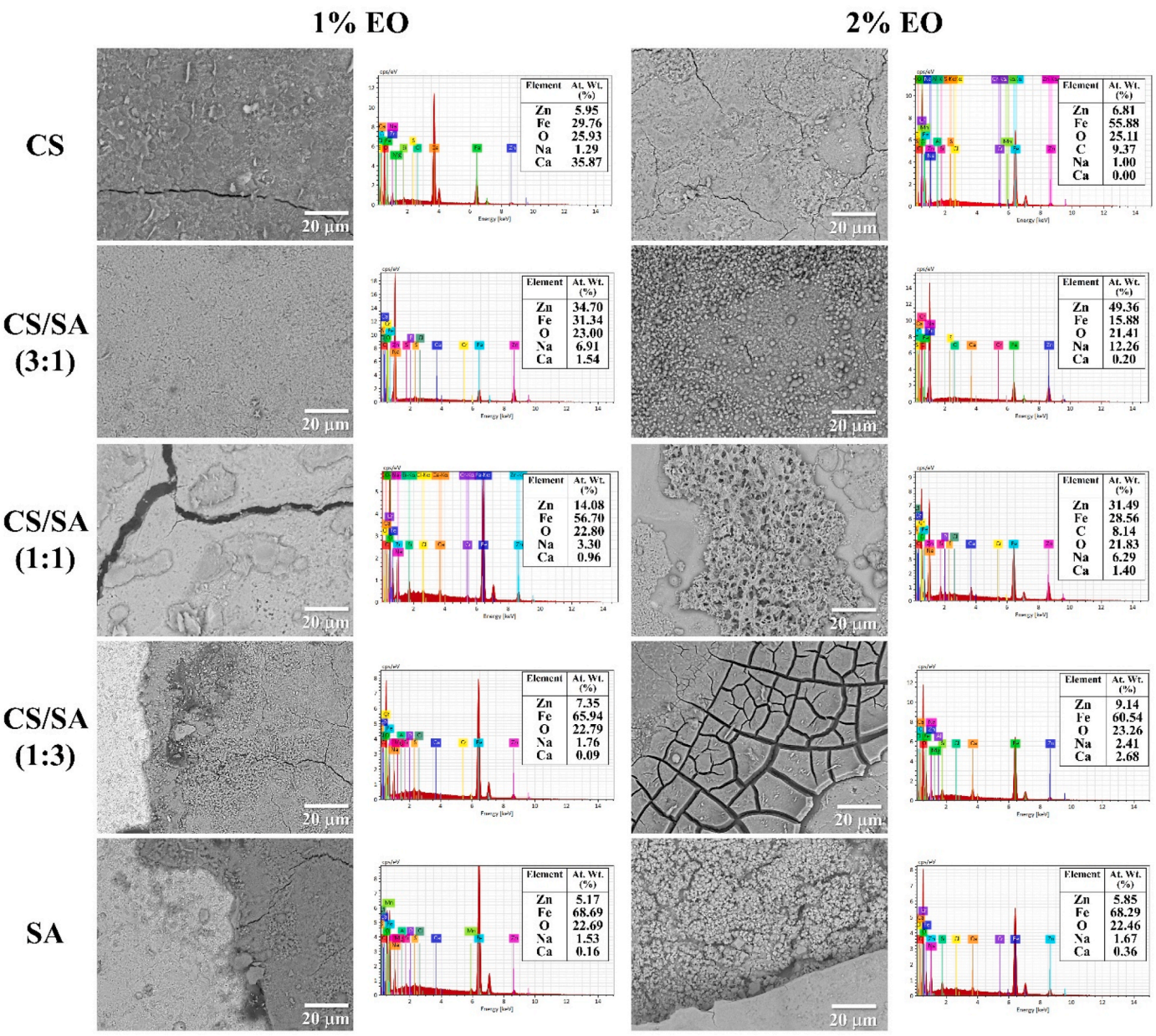

Fig. 9. SEM micrographs and the corresponding EDS spectra of elemental composition of the hydrogel-coated surface when removing the hydrogel, after 120 days of immersion in non-sterile wastewater.

stability, likely through stronger ionic cross-linking (mediated by Ca^{2+}), enhanced hydrophobic interactions, or reduced hydrolytic susceptibility. While degradation was quantitatively assessed, complementary evaluation of mechanical properties is needed to fully characterize the material's durability. Overall, the results emphasize the critical influence of polymer ratio and additive composition in designing cryogels for long-term environmental or biomedical applications.

To contextualize our findings, key parameters, such as encapsulation efficiency, degradation stability, and antibacterial activity, were compared with related systems (Table 3). The CS/SA (3:1) cryogel incorporating *Satureja montana* EO and *Monarda didyma* hydrolate shows notable advantages. Unlike several nanoparticle-based systems (e.g., ZnO, TiO_2 or Au composites [19,64,88]), which often lack encapsulation data or degrade rapidly, the present formulation achieved high encapsulation efficiency (78.7 %) and moderate mass loss (58.1 ± 1.0 %) over four months. This compares favorably with similar natural systems (e.g., 45–70 % EE for nettle oil hydrogels [89]) and outperforms synthetic matrices with limited stability (e.g., 17 % degradation in 21 days for curcumin-loaded hybrids [17]). The broad-spectrum antimicrobial activity, rated from "very high" to "excellent," aligns with inorganic-enhanced formulations, confirming the efficacy of natural bioactives without reliance on metal-based agents. Overall, this cryogel system offers a sustainable and multifunctional alternative for biomedical and environmental applications.

4. Conclusion

This study successfully developed and characterized chitosan-sodium alginate (CS/SA) hydrogel coatings incorporating natural additives, demonstrating strong antibacterial and anticorrosion potential. The formulation with a CS:SA ratio of 3:1 and 2 % *Satureja montana* essential oil (EO), particularly in combination with *Monarda didyma* hydrolate, exhibited the most effective performance. This combination provided superior encapsulation efficiency, reduced EO leakage, and

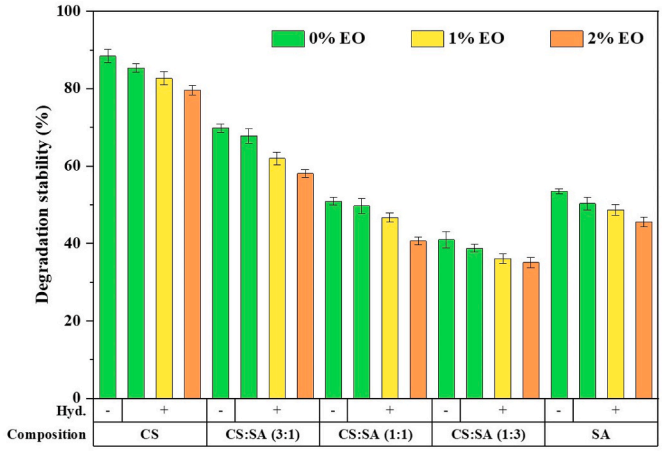

Fig. 10. The degradation stability of the cryogels, with (+) and without (−) hydrolate (Hyd.) and various EO proportions.

Table 3
Comparison table of crucial properties for related works.

Materials (components)	EE (%)	Degradation Stability	Antibacterial efficacy **	Ref.
CS/SA (3:1) + *Satureja montana* EO + *Monarda didyma* hydrolate	78.7 %	58.1 ± 1.0	**Very high:** *S. aureus* **High:** *P. aeruginosa* **Excellent:** APB and BTR	This work
PVP + Curcumin + Gold nanoparticles	/	17 % degradation of curcumin/21 days	**Excellent:** *E. coli*	[17]
SA + *Citronella (lemongrass)* EO + ZnO nanoparticles	/	60 %	**Excellent:** *E. coli*, *S. Typhi*, *B. cereus* and *S. aureus*)	[19]
Amphiphilic sodium alginate-polylysine + Thymol Oligomeric tannic acid	/	/	**Excellent:** *E. coli* and *S. aureus*	[20]
Creatine-gelatin + *Zataria multiflora* EO + TiO_2 nanoparticles	98.8 %	/	**Excellent:** *P. eruginosa, S. aureus, E. coli* and *Candida* sp	[64]
Calcium alginate + Au nanoparticles ZIF-8/$Ti_3C_2T_x$	/	/	**Excellent:** *E. coli* and *S. aureus*	[88]
CS/SA (1:1) + Nettle oil and extract	45–70 %	/	**Excellent:** *P. aeruginosa, S. aureus* and *E. coli*	[89]
HEMA + *hydroxylated polymeric linolenic acid*	/	/	**Very high:** *P. aeruginosa* and *S. aureus* **Moderate:** *Saccharomyces cerevisiae* yeast	[90]

* The antibacterial activity is expressed by the percentage reduction in *S. aureus* and *P. aeruginosa* growth: low (minimal inhibition); moderate (20–40 % bacterial reduction); high (40–60 %); Very High (60–85 %); excellent (>85 %).

enhanced protective properties. The synergistic interactions between chitosan and alginate reinforced the hydrogel network, while the EO and hydrolate contributed antimicrobial and hydrophobic effects.

Structural analysis revealed that higher alginate content improved porosity, while EO inclusion promoted densification and sheet stacking, enhancing the tunability of the hydrogel. Antibacterial tests showed significant inhibition of *Staphylococcus aureus*, *Pseudomonas aeruginosa*, and biocorrosion-inducing bacteria, attributed to the bioactive and membrane-disrupting effects of the EO and hydrolate. Corrosion assays demonstrated that these hydrogels reduced biofilm formation and metal degradation, evidenced by minimized weight loss, reduced surface damage, and high zinc retention on coated samples.

Overall, this work highlights the versatility of CS/SA hydrogels enriched with natural additives for sustainable material protection and microbial control. These findings provide a foundation for advancing polymer-based coatings in industrial and environmental applications, with future studies focusing on long-term durability and scalability for broader use.

CRediT authorship contribution statement

Imane Haddadou: Writing – original draft, Visualization, Validation, Methodology, Investigation, Formal analysis, Conceptualization. **Amina Ami:** Writing – review & editing, Methodology, Investigation, Conceptualization. **Jonathan Gagnon:** Writing – review & editing, Investigation, Funding acquisition. **Claudiane M. Ouellet-Plamondon:** Conceptualisation, Methodology, Investigation, Validation, Supervision, Resources, Writing – review & editing, Project administration, Funding acquisition

Declaration of competing interest

The authors declare that they have no known competing financial interests or personal relationships that could appear to have influenced the work reported in this paper.

The authors have no relevant financial or non-financial interests to disclose.

Acknowledgment

The authors would like to acknowledge the financial support from the Centre québécois sur les matériaux fonctionnels/Québec Centre for Advanced Materials (CQMF/QCAM) from Fonds de recherche du Québec–Nature et Technologies (FRQNT) and the Canada Research on Sustainable Multifunctional Construction Materials (CRC-2019-00074).

Appendix A. Supplementary data

Supplementary data to this article can be found online at https://doi.org/10.1016/j.mtchem.2025.102719.

Data availability

No data was used for the research described in the article.

References

[1] D.A. Gyles, et al., A review of the designs and prominent biomedical advances of natural and synthetic hydrogel formulations, Eur. Polym. J. 88 (2017) 373–392, https://doi.org/10.1016/j.eurpolymj.2017.01.027.
[2] E.M. Ahmed, Hydrogel: preparation, characterization, and applications: a review, J. Adv. Res. 6 (2) (2015) 105–121, https://doi.org/10.1016/j.jare.2013.07.006.
[3] F. Altaf, et al., Synthesis and characterization of PVA/starch hydrogel membranes incorporating essential oils aimed to be used in wound dressing applications, J. Polym. Environ. 29 (1) (2021) 156–174, https://doi.org/10.1007/s10924-020-01866-w.
[4] S. Aswathy, U. Narendrakumar, I. Manjubala, Commercial hydrogels for biomedical applications, Heliyon 6 (4) (2020) e03719, https://doi.org/10.1016/j.heliyon.2020.e03719.
[5] N. Yuan, et al., Chitosan, alginate, hyaluronic acid and other novel multifunctional hydrogel dressings for wound healing: a review, Int. J. Biol. Macromol. 240 (2023) 124321, https://doi.org/10.1016/j.ijbiomac.2023.124321.
[6] L. Qi, et al., Preparation and antibacterial activity of chitosan nanoparticles, Carbohydr. Res. 339 (16) (2004) 2693–2700, https://doi.org/10.1016/j.carres.2004.09.007.
[7] E.S. de Alvarenga, Characterization and properties of chitosan, Biotechnol. Biopolym. 91 (2011) 48–53.

[8] S.-H. Chang, et al., pH Effects on solubility, zeta potential, and correlation between antibacterial activity and molecular weight of chitosan, Carbohydr. Polym. 134 (2015) 74–81, https://doi.org/10.1016/j.carbpol.2015.07.072.
[9] M. Rinaudo, Chitin and chitosan: properties and applications, Prog. Polym. Sci. 31 (7) (2006) 603–632, https://doi.org/10.1016/j.progpolymsci.2006.06.001.
[10] S. Thakur, et al., Recent progress in sodium alginate based sustainable hydrogels for environmental applications, J. Clean. Prod. 198 (2018) 143–159, https://doi.org/10.1016/j.jclepro.2018.06.259.
[11] I. Cruz-Maya, et al., 13 - ionotropic cross-linked polymeric beads for drug delivery and in vitro applications, in: A.K. Nayak, M.S. Hasnain (Eds.), Ionotropic Cross-Linking of Biopolymers, Elsevier, 2024, pp. 387–416, https://doi.org/10.1016/B978-0-323-96116-5.00020-X.
[12] M. Saberian, et al., How the combination of alginate and chitosan can fabricate a hydrogel with favorable properties for wound healing, Heliyon 10 (11) (2024) e32040, https://doi.org/10.1016/j.heliyon.2024.e32040.
[13] S. Jana, S. Jana. Alginate Biomaterial: Drug Delivery Strategies and Biomedical Engineering, Springer Nature, 2023, https://doi.org/10.1007/978-981-19-6937-9.
[14] W.L.C. Ribeiro, et al., Activity of chitosan-encapsulated Eucalyptus staigeriana essential oil on Haemonchus contortus, Exp. Parasitol. 135 (1) (2013) 24–29, https://doi.org/10.1016/j.exppara.2013.05.014.
[15] S. Gholamian, M. Nourani, N. Bakhshi, Formation and characterization of calcium alginate hydrogel beads filled with cumin seeds essential oil, Food Chem. 338 (2021) 128143, https://doi.org/10.1016/j.foodchem.2020.128143.
[16] V.P. Brahmkhatri, et al., Curcumin nanoconjugate inhibits aggregation of N-terminal region (Aβ-16) of an amyloid beta peptide, New J. Chem. 42 (24) (2018) 19881–19892, https://doi.org/10.1039/C8NJ03541E.
[17] P. Rananaware, et al., Polymeric curcumin nanospheres for lysozyme aggregation inhibition, antibacterial, and wound healing applications, Environ. Sci. Pollut. Control Ser. 31 (34) (2024) 46625–46640, https://doi.org/10.1007/s11356-023-29160-x.
[18] Q. Li, et al., AgNPs-loaded chitosan/sodium alginate hydrogel film by in-situ green reduction with tannins for enhancing antibacterial activity, Mater. Today Commun. 38 (2024) 107927, https://doi.org/10.1016/j.mtcomm.2023.107927.
[19] L. Motelica, et al., Biodegradable alginate films with ZnO nanoparticles and citronella essential oil—a novel antimicrobial structure, Pharmaceutics 13 (2021), https://doi.org/10.3390/pharmaceutics13071020.
[20] F. Jin, et al., Amphiphilic sodium alginate-polylysine hydrogel with high antibacterial efficiency in a wide pH range, Carbohydr. Polym. 299 (2023) 120195, https://doi.org/10.1016/j.carbpol.2022.120195.
[21] A. Ehterami, et al., Chitosan/alginate hydrogels containing Alpha-tocopherol for wound healing in rat model, J. Drug Deliv. Sci. Technol. 51 (2019) 204–213, https://doi.org/10.1016/j.jddst.2019.02.032.
[22] A.L.R. Pires, et al., Towards wound dressings with improved properties: effects of poly (dimethylsiloxane) on chitosan-alginate films loaded with thymol and beta-carotene, Mater. Sci. Eng. C 93 (2018) 595–605, https://doi.org/10.1016/j.msec.2018.08.005.
[23] H. Wang, S. Huang, X. Xu, Calcium alginate reinforced zwitterionic double network hydrogel with mechanical robustness and antimicrobial activity for freshwater shrimp spoilage detection, Food Res. Int. 200 (2025) 115483, https://doi.org/10.1016/j.foodres.2024.115483.
[24] S. Catty, Hydrosols: the Next Aromatherapy: Inner Traditions/Bear, Co, 2001.
[25] R. Adams, Identification of Essential Oils Components by Gas Chromatography Mass Spectroscopy, Allured Pubishing Corporation, Carol Stream, Illinois, USA, 2007, 4th edition.
[26] M.A. Hanif, et al., Essential oils, in: S. Malik (Ed.), Essential Oil Research, Springer, 2019, pp. 3–17, https://doi.org/10.1007/978-3-030-16546-8_1.
[27] P. Rananaware, P. Pandit, V. Brahmkhatri, Gold nanoparticle encapsulated hybrid MOF: synthesis, characterization, and co-drug delivery of 5-fluorouracil and curcumin, Discover Nano 19 (1) (2024) 201, https://doi.org/10.1186/s11671-024-04152-z.
[28] K. Torpol, et al., Optimising chitosan–pectin hydrogel beads containing combined garlic and holy basil essential oils and their application as antimicrobial inhibitor, Int. J. Food Sci. Technol. 54 (6) (2019) 2064–2074, https://doi.org/10.1111/ijfs.14107.
[29] A. Moukhles, et al., Chemical composition, in vitro antibacterial activity and corrosion inhibition of essential oil and hydrolat extract from aerial parts of thymbra capitata (L.) cav harvested at Northern Morocco, J. Essen. Oil. Bearing. Plant. 23 (2) (2020) 375–389, https://doi.org/10.1080/0972060X.2020.1760147.
[30] S. D'Amato, et al., Hydrosols: biological activity and potential as antimicrobials for food applications, Food Control 86 (2018) 126–137, https://doi.org/10.1016/j.foodcont.2017.10.030.
[31] D. Šilha, et al., Chemical composition of natural hydrolates and their antimicrobial activity on arcobacter-like cells in comparison with other microorganisms, Molecules 25 (23) (2020), https://doi.org/10.3390/molecules25235654.
[32] Y. Guo, et al., Advanced functional chitosan-based nanocomposite materials for performance-demanding applications, Prog. Polym. Sci. (2024) 101872, https://doi.org/10.1016/j.progpolymsci.2024.101872.
[33] A. Gupta, R. Prasad, Antimicrobials in Pharmaceutical and Medicinal Research, CRC Press, 2023, https://doi.org/10.1201/9781003268932.
[34] T.E. Perez, Corrosion in the oil and gas industry: an increasing challenge for materials, Jom 65 (8) (2013) 1033–1042, https://doi.org/10.1007/s11837-013-0675-3.
[35] M. Mostaghimi, M. Majdinasab, S.M.H. Hosseini, Characterization of alginate hydrogel beads loaded with thyme and clove essential oils nanoemulsions, J. Polym. Environ. 30 (4) (2022) 1647–1661, https://doi.org/10.1007/s10924-021-02298-w.
[36] W.L. Low, et al., Ionically Crosslinked Chitosan Hydrogels for the Controlled Release of Antimicrobial Essential Oils and Metal Ions for Wound Management Applications, Medicines 3 (1) (2016) 8, https://doi.org/10.3390/medicines3010008.
[37] Z. Hu, et al., Antibacterial and anticorrosive hydrogel coating based on complementary functions of sodium alginate and g-C3N4, Molecules 29 (17) (2024) 4192, https://doi.org/10.3390/molecules29174192.
[38] W. Mantooth, The Native American Medical Herbalism Dictionary: Proven Natural Herbal Remedies to Stop Using Chemical Drugs and Heal Common Ailments with Sacred Medicinal Plants to Eradicate Diseases Naturally, Independently Published, 2020.
[39] L. Finetti, et al., *Monarda didyma* hydrolate affects the survival and the behaviour of *Drosophila suzukii*, Insects 13 (3) (2022) 280, https://doi.org/10.3390/insects13030280.
[40] M. Di Vito, et al., Is the antimicrobial activity of hydrolates lower than that of essential oils? Antibiotics 10 (1) (2021) 88, https://doi.org/10.3390/antibiotics10010088.
[41] Z. Pilić, I. Dragičević, I. Martinović, The anti-corrosion behaviour of *Satureja Montana L.* extract on iron in NaCl solution, Open Chem. 17 (1) (2019) 1087–1094, https://doi.org/10.1515/chem-2019-0126.
[42] B.A. An, et al., Iron to gas: versatile multiport flow-column revealed extremely high corrosion potential by methanogen-induced microbiologically influenced corrosion (Mi-MIC), Front. Microbiol. 11 (2020) 527, https://doi.org/10.3389/fmicb.2020.00527.
[43] G.C. Feyzioglu, F. Tornuk, Development of chitosan nanoparticles loaded with summer savory (*Satureja hortensis* L.) essential oil for antimicrobial and antioxidant delivery applications, Lebensm. Wiss. Technol. 70 (2016) 104–110, https://doi.org/10.1016/j.lwt.2016.02.037.
[44] A. Zhang, et al., Fabrication and characterization of bamboo shoot cellulose/sodium alginate composite aerogels for sustained release of curcumin, Int. J. Biol. Macromol. 192 (2021) 904–912, https://doi.org/10.1016/j.ijbiomac.2021.10.027.
[45] K. Ganesan, et al., Review on the production of polysaccharide aerogel particles, Materials 11 (11) (2018) 2144, https://doi.org/10.3390/ma11112144.
[46] D.N. Carvalho, et al., Marine collagen-chitosan-fucoidan cryogels as cell-laden biocomposites envisaging tissue engineering, Biomed. Mater 15 (5) (2020) 055030, https://doi.org/10.1088/1748-605X/ab9f04.
[47] ASTM, E2149: Standard Test Method for Determining the Antimicrobial Activity of Immobilized Antimicrobial Agents under Dynamic Contact Conditions, 2010.
[48] S. Rathee, et al., Smart alginate nanomaterials: revolutionizing food across delivery, preservation, packaging, safety, and waste upcycling, Carbohydr. Polym. Technol. Appl. 8 (2024) 100568, https://doi.org/10.1016/j.carpta.2024.100568.
[49] N.A. Gorshkova, et al., Influence of the structure of alginate-chitosan materials on the kinetics of usnic acid release, Appl. Biochem. Microbiol. 58 (2) (2022) 110–117, https://doi.org/10.1134/S0003683822020089.
[50] J. Pan, et al., Enhanced physical and antimicrobial properties of alginate/chitosan composite aerogels based on electrostatic interactions and noncovalent crosslinking, Carbohydr. Polym. 266 (2021) 118102, https://doi.org/10.1016/j.carbpol.2021.118102.
[51] I. Syed, S. Garg, P. Sarkar, Polymeric Gels, in: K. Pal, I. Banerjee (Eds.), Entrapment of Essential Oils in Hydrogels for Biomedical Applications, 5, Woodhead Publishing, 2018, pp. 125–141, https://doi.org/10.1016/B978-0-08-102179-8.00005-3.
[52] N. Bölgen, et al., Development of *Hypericum perforatum* oil incorporated antimicrobial and antioxidant chitosan cryogel as a wound dressing material, Int. J. Biol. Macromol. 161 (2020) 1581–1590, https://doi.org/10.1016/j.ijbiomac.2020.08.056.
[53] M.V. Dinu, et al., Physically cross-linked chitosan/dextrin cryogels entrapping *Thymus vulgaris* essential oil with enhanced mechanical, antioxidant and antifungal properties, Int. J. Biol. Macromol. 184 (2021) 898–908, https://doi.org/10.1016/j.ijbiomac.2021.06.068.
[54] P. Lertsutthiwong, et al., Preparation of alginate nanocapsules containing turmeric oil, Carbohydr. Polym. 74 (2) (2008) 209–214, https://doi.org/10.1016/j.carbpol.2008.02.009.
[55] R. Essid, et al., Assessment of nanoencapsulated *Syzygium aromaticum* essential oil in chitosan-alginate nanocareer as a new antileishmanial and antimicrobial system approach, J. Polym. Environ. 31 (11) (2023) 4784–4800, https://doi.org/10.1007/s10924-023-02911-0.
[56] X. Meng, et al., Chitosan/alginate/hyaluronic acid polyelectrolyte composite sponges crosslinked with genipin for wound dressing application, Int. J. Biol. Macromol. 182 (2021) 512–523, https://doi.org/10.1016/j.ijbiomac.2021.04.044.
[57] T. Kopač, R. Ambrožič, Tailored alginate and chitosan hydrogels: structural control and functional applications via copper-based electrodeposition, Int. J. Biol. Macromol. 308 (2025) 142476, https://doi.org/10.1016/j.ijbiomac.2025.142476.
[58] G. Lawrie, et al., Interactions between alginate and chitosan biopolymers characterized using FTIR and XPS, Biomacromolecules 8 (8) (2007) 2533–2541, https://doi.org/10.1021/bm070014y.
[59] D. Kulig, et al., Study on alginate–chitosan complex formed with different polymers ratio, Polymers 8 (5) (2016) 167, https://doi.org/10.3390/polym8050167.
[60] A. Rezaei, H. Ehtesabi, Fabrication of alginate/chitosan nanocomposite sponges using green synthesized carbon dots as potential wound dressing, Mater. Today Chem. 24 (2022) 100910, https://doi.org/10.1016/j.mtchem.2022.100910.
[61] Y. Li, et al., Durable, cost-effective and superhydrophilic chitosan-alginate hydrogel-coated mesh for efficient oil/water separation, Carbohydr. Polym. 226 (2019) 115279, https://doi.org/10.1016/j.carbpol.2019.115279.
[62] M.P.M. Costa, et al., Interaction of polyelectrolyte complex between sodium alginate and chitosan dimers with a single glyphosate molecule: a DFT and NBO

study, Carbohydr. Polym. 198 (2018) 51–60, https://doi.org/10.1016/j.carbpol.2018.06.052.
[63] L. Zhu, et al., Tannic acid modified keratin/sodium alginate/carboxymethyl chitosan biocomposite hydrogels with good mechanical properties and swelling behavior, Sci. Rep. 14 (1) (2024) 12864, https://doi.org/10.1038/s41598-024-63186-6.
[64] M.H. Hashempur, et al., Enrichment of creatine-gelatin cryogel with *Zataria multiflora* essential oil and titanium dioxide nanoparticles as a potential wound dressing, Mater. Today Chem. 38 (2024) 102069, https://doi.org/10.1016/j.mtchem.2024.102069.
[65] S. Ariaeenejad, E. Motamedi, Improved saccharification of rice straw by removing phenolic compounds using a stable immobilized metagenome-derived laccase on sodium alginate-based hydrogel, Biochem. Eng. J. 198 (2023) 109021, https://doi.org/10.1016/j.bej.2023.109021.
[66] A. Tripathi, A. Kumar, Multi-featured macroporous agarose–alginate cryogel: synthesis and characterization for bioengineering applications, Macromol. Biosci. 11 (1) (2011) 22–35, https://doi.org/10.1002/mabi.201000286.
[67] C. Chartier, et al., Tuning the properties of porous chitosan: aerogels and cryogels, Int. J. Biol. Macromol. 202 (2022) 215–223, https://doi.org/10.1016/j.ijbiomac.2022.01.042.
[68] T.M.A. Henderson, et al., Cryogels for biomedical applications, J. Mater. Chem. B 1 (21) (2013) 2682–2695, https://doi.org/10.1039/C3TB20280A.
[69] C.S. Tavares, et al., Hydrolates: a review on their volatiles composition, biological properties and potential uses, Phytochem. Rev. 21 (5) (2022) 1661–1737, https://doi.org/10.1007/s11101-022-09803-6.
[70] J. Oliveira-Fernandes, et al., Satureja Montana and Mentha pulegium essential oils' antimicrobial properties against Pseudomonas syringae pv. actinidiae and elicitor potential through the modulation of kiwifruit hormonal defenses, Microbiol. Res. 277 (2023) 127490, https://doi.org/10.1016/j.micres.2023.127490.
[71] A. Maccelli, L. Satureja montana, et al., Essential oils: chemical profiles/phytochemical screening, antimicrobial activity and O/W NanoEmulsion formulations, Pharmaceutics 12 (1) (2020) 7, https://doi.org/10.3390/pharmaceutics12010007.
[72] J.D.C. Santos, et al., Chemical composition and antimicrobial activity of Satureja Montana byproducts essential oils, Ind. Crop. Prod. 137 (2019) 541–548, https://doi.org/10.1016/j.indcrop.2019.05.058.
[73] D.I. Bezbradica, et al., Composition and antimicrobial activity of essential oil of *Satureja Montana* L. collected in Serbia and Montenegro, J. Essent. Oil Res. 17 (4) (2005) 462–465, https://doi.org/10.1080/10412905.2005.9698965.
[74] C. Karthik, D.G. Caroline, S. Pandi Prabha, Nanochitosan augmented with essential oils and extracts as an edible antimicrobial coating for the shelf life extension of fresh produce: a review, Polym. Bull. 79 (10) (2022) 8009–8032, https://doi.org/10.1007/s00289-021-03901-9.
[75] K. Sharma, M. Goyat, P. Vishwakarma, Synthesis of Polymer Nano-composite coatings as corrosion inhibitors: a quick review, in: IOP Conference Series: Materials Science and Engineering, IOP Publishing, 2020, https://doi.org/10.1088/1757-899X/983/1/012016.
[76] A. Gallegos-Melgar, et al., Potentiodynamic polarization performance of a novel composite coating system of Al_2O_3/chitosan-sodium alginate, applied on an aluminum AA6063 alloy for protection in a chloride ions environment, Coatings 10 (1) (2020) 45, https://doi.org/10.3390/coatings10010045.
[77] T. Liu, et al., Development and characterization of novel active chitosan films containing fennel and peppermint essential oils, Coatings 10 (10) (2020) 936, https://doi.org/10.3390/coatings10100936.
[78] L.L. Shreir, Corrosion: Metal/environment Reactions, Newnes, 2013.
[79] R. Javaherdashti, in: Microbiologically influenced corrosion (MIC), Microbiologically Influenced Corrosion: an Engineering Insight, Springer, London: London, 2008, pp. 29–71, https://doi.org/10.1007/978-3-319-44306-5_4.
[80] D. Xu, T. Gu, D.R. Lovley, Microbially mediated metal corrosion, Nat. Rev. Microbiol. 21 (11) (2023) 705–718, https://doi.org/10.1038/s41579-023-00920-3.
[81] I.B. Beech, J. Sunner, Biocorrosion: towards understanding interactions between biofilms and metals, Curr. Opin. Biotechnol. 15 (3) (2004) 181–186, https://doi.org/10.1016/j.copbio.2004.05.001.
[82] R. Abka-khajouei, et al., Structures, properties and applications of alginates, Mar. Drugs 20 (2022), https://doi.org/10.3390/md20060364.
[83] Y. Duan, et al., Chitosan-sodium alginate-based coatings for self-strengthening anticorrosion and antibacterial protection of titanium substrate in artificial saliva, Int. J. Biol. Macromol. 184 (2021) 109–117, https://doi.org/10.1016/j.ijbiomac.2021.06.042.
[84] S.M.Z. Hossain, S.A. Razzak, M.M. Hossain, Application of essential oils as green corrosion inhibitors, Arabian J. Sci. Eng. 45 (9) (2020) 7137–7159, https://doi.org/10.1007/s13369-019-04305-8.
[85] K.Y. Lee, D.J. Mooney, Alginate: properties and biomedical applications, Prog. Polym. Sci. 37 (1) (2012) 106–126, https://doi.org/10.1016/j.progpolymsci.2011.06.003.
[86] G. Rassu, et al., Composite chitosan/alginate hydrogel for controlled release of deferoxamine: a system to potentially treat iron dysregulation diseases, Carbohydr. Polym. 136 (2016) 1338–1347, https://doi.org/10.1016/j.carbpol.2015.10.048.
[87] S. Vakilian, et al., A competitive nature-derived multilayered scaffold based on chitosan and alginate, for full-thickness wound healing, Carbohydr. Polym. 262 (2021) 117921, https://doi.org/10.1016/j.carbpol.2021.117921.
[88] Z. Fang, et al., Dual photothermal-photocatalytic Au@ZIF-8/Ti3C2Tx nanocomposite for enhanced solar steam sterilization and biofouling-resistant hydrogel membrane, Mater. Today Chem. 43 (2025) 102467, https://doi.org/10.1016/j.mtchem.2024.102467.
[89] P. Salehi, et al., Chitosan/alginate hydrogel adorned with nanoemulsions for potential wound healing: fabrication, characterization, and biocompatibility evaluation, Alex. Eng. J. 117 (2025) 45–52, https://doi.org/10.1016/j.aej.2024.12.101.
[90] A. Alli, et al., Hydroxylated polymeric linolenic acid containing cytocompatible cryogels with antibiofilm activities, Mater. Today Chem. 44 (2025) 102602, https://doi.org/10.1016/j.mtchem.2025.102602.